Sussex Research Online

A TPD and RAIRS comparison of the low temperature behavior of benzene, toluene, and xylene on graphite

Article (Accepted Version)

Salter, Tara L, Stubbing, James W, Brigham, Lorna and Brown, Wendy A (2018) A TPD and RAIRS comparison of the low temperature behavior of benzene, toluene, and xylene on graphite. The Journal of Chemical Physics, 149 (164705). pp. 1-11. ISSN 0021-9606

This version is available from Sussex Research Online: http://sro.sussex.ac.uk/id/eprint/79577/

This document is made available in accordance with publisher policies and may differ from the published version or from the version of record. If you wish to cite this item you are advised to consult the publisher's version. Please see the URL above for details on accessing the published version.

Copyright and reuse:
Sussex Research Online is a digital repository of the research output of the University.

Copyright and all moral rights to the version of the paper presented here belong to the individual author(s) and/or other copyright owners. To the extent reasonable and practicable, the material made available in SRO has been checked for eligibility before being made available.

Copies of full text items generally can be reproduced, displayed or performed and given to third parties in any format or medium for personal research or study, educational, or not-for-profit purposes without prior permission or charge, provided that the authors, title and full bibliographic details are credited, a hyperlink and/or URL is given for the original metadata page and the content is not changed in any way.

http://sro.sussex.ac.uk

A TPD and RAIRS comparison of the low temperature surface behaviour of benzene, toluene and xylene on graphite

Tara L. Salter, James W. Stubbing, Lorna Brigham, Wendy A. Brown*

Department of Chemistry, School of Life Sciences, University of Sussex, Falmer, Brighton BN1 9QJ, UK

*Corresponding author: w.a.brown@sussex.ac.uk

Abstract

The first comparative study of the surface behaviour of four small aromatic molecules, benzene, toluene, *p*-xylene and o-xylene, adsorbed on graphite at temperatures ≤ 30 K, is presented. Intermolecular interactions are shown to be important in determining the growth of the molecules on the graphite surface at low (monolayer) exposures. Repulsive intermolecular interactions dominate the behaviour of benzene and toluene. In contrast, stronger interactions with the graphite surface are observed for the xylene isomers, with islanding observed for *o*-xylene. Multilayer desorption temperatures and energies increase with the size of the molecule, ranging from 45.5 to 59.5 kJ mol^{-1} for benzene and *p*-xylene respectively. Reflection absorption infrared spectroscopy gives insight into the effects of thermal processing on the ordering of the molecules. Multilayer benzene, *p*-xylene and *o*-xylene form crystalline structures following annealing of the ice. However, we do not observe an ordered structure for toluene in this study. The ordering of *p*-xylene shows a complex relationship dependent on both the annealing temperature and exposure.

Introduction

Benzene, toluene and xylene are a family of aromatic molecules, shown in figure 1. The addition, and relative position, of methyl groups on the benzene ring affects both the size and shape of the molecule as well as its polarity. Benzene and *p*-xylene are apolar, whereas toluene and *o*-xylene have dipole moments of 0.36 and 0.64 Debye, respectively.[1] These small differences between the molecules have a noticeable effect on their properties and behaviour.

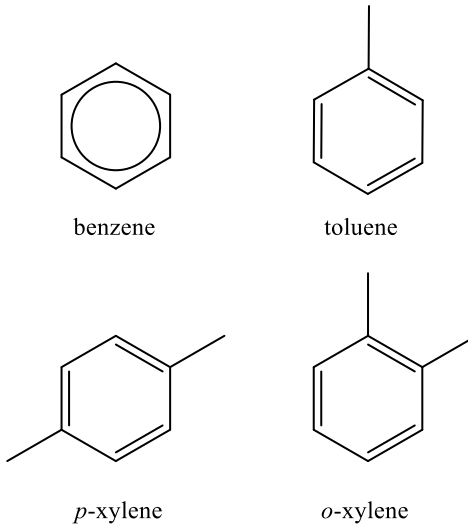

Figure 1. *Molecular structures of benzene, toluene, p-xylene and o-xylene.*

Benzene and its methyl-substituted derivatives are important in a wide range of fields on Earth and in space. On Earth, these molecules are pollutants that are released in anthropogenic emissions from combustion processes and industrial solvents.[2,3] They contribute to the formation of soot particles,[4–6] and can also react with other species to form ozone and secondary organic aerosols (SOA).[7–10] Various methods have been used to control the emission of these small aromatics and one of the most efficient procedures is removal via adsorption onto porous surfaces, including those of a carbonaceous nature.[11–14]

Benzene, toluene and xylene also have importance in various regions of space. For example, benzene has been detected in protoplanetary nebulae[15,16] and formation routes of toluene and xylene in interstellar clouds have been postulated.[17,18] Small aromatic molecules are also of interest because of

their potential as building blocks of larger polycyclic aromatic hydrocarbons (PAHs).[19] PAHs are ubiquitous in space and are thought to account for up to 20% of the galactic carbon, as well as being intermediates in the formation of carbonaceous dust grains. [20,21] In the interstellar medium (ISM), icy mantles form on these dust grains at low temperatures (10-20 K), and hence studying the low temperature adsorption of ices on dust grains provides insight into these processes. Small aromatic molecules, such as benzene, toluene and xylene, are particularly interesting in this regard as they offer a simplified model for studying the adsorption of PAHs in the laboratory.

There have been several experimental studies investigating the behaviour of benzene on surfaces at the very low temperatures relevant to astrochemistry. Temperature programmed desorption (TPD), high resolution electron energy loss spectroscopy (HREELS), metastable impact electron spectroscopy (MIES) and infrared spectroscopy have been utilised to study the structural orientation and desorption of benzene ices. These techniques have demonstrated that on Ru(001)[22–24] and Mo(100),[24] benzene first chemisorbs before forming three distinct physisorbed phases, including a metastable state at intermediate coverages. In contrast, experiments on Cu(111) identified the formation of a stable bilayer between monolayer and multilayer benzene adsorption.[25] TPD studies of benzene on non-metallic surfaces gave differing results at low coverages. Benzene adsorbed on highly oriented pyrolytic graphite (HOPG),[26,27] carbon nanotubes (CNTs)[26] and graphene covered Pt(111)[28] showed well-resolved monolayer desorption peaks. However other work on CNTs,[29] SiO_2 [30,31] and graphene coated metal and SiO_2 supports[32,33] shows repulsive interactions between adsorbates at low exposures and a coverage dependent binding energy.

There have been extensive studies on the higher temperature adsorption of benzene, with particular relevance to its application in catalysis, see for example refs [34–36]. Previous work has also studied the higher temperature adsorption of toluene and xylene on different surfaces including graphite, zeolites and silica-based adsorbents.[37–40] Less experimental data is available on toluene in the temperature regime (≤ 30 K) relevant to the investigations described here. TPD studies have been performed on

graphite, examining the sub-monolayer behaviour of toluene adsorbed at ~ 20 K.[26] Metal surfaces have also been utilised to examine the thermal behaviour of toluene adsorbed on Ru(001) at 120 K.[41] A reflection infrared absorption spectroscopy (RAIRS) study of toluene adsorbed on Ni(111) at 110 K showed that it is weakly adsorbed on the substrate.[42] TPD studies have also been conducted to study xylene adsorbed above 150 K. In particular, *p*-xylene and *o*-xylene were adsorbed on Pt(111)[43] and partially deuterated xylene isomers were studied on Ni(111) and Ni(100).[44] No previous RAIRS studies have been reported for xylene. Theoretical studies of the physisorption of methylbenzenes on graphene, using density functional theory with the van der Waals functional (vdW-DF), have calculated adsorption energies for all four molecules.[45]

In order to understand the effects of size and polarity on the adsorption and desorption behaviour of benzene, toluene and xylene on HOPG, we have performed a detailed comparative experimental study using RAIRS and TPD. This is the first study to our knowledge that comprehensively examines the adsorption of toluene and xylene isomers on HOPG at very low temperatures, ~30 K. Exposure dependent TPD studies highlight the differences between the desorption behaviours of these molecules. Monolayer and multilayer desorption kinetic parameters, including desorption energies, have been determined for each molecule from the TPD data. RAIRS annealing experiments have also been performed and these provide complementary information concerning the structural ordering of the ices with increasing temperature.

Experimental

Experiments were carried out in two separate ultra-high vacuum (UHV) chambers, with base pressures of $\leq 2 \times 10^{-10}$ mbar. Benzene and toluene data were recorded in chamber (1) and xylene data were measured in chamber (2). Each chamber is equipped with a closed-cycle helium refrigerator (SHI-APD) which allows the sample to be cooled to a base temperature of 25 K (chamber 1) or 30 K (chamber 2) as measured by an N-type or E-type thermocouple, respectively. A HOPG surface was used as a carbonaceous dust grain model in both cases. The HOPG surface was cleaned before each experiment

by annealing to 250 K and surface cleanliness was confirmed by the absence of any desorption products in TPD experiments with no dose.

Benzene (Sigma Aldrich, purity 99.9%), toluene (Sigma Aldrich, purity 99.9%), *p*-xylene (Sigma Aldrich, purity 99.5%) and *o*-xylene (Sigma Aldrich, purity 99.5%) were purified by repeated freeze-pump-thaw cycles. Ices were grown on the HOPG surface via background deposition using high-precision leak valves. All exposures are given in Langmuir (L_m) where 1 $L_m = 10^{-6}$ mbar s. Despite differences between the chambers, calculations show that similar exposures in both chambers give comparable coverages of the adsorbates on the HOPG surface. To confirm this, it was necessary to convert exposure in L_m to coverage to allow a comparison between the data for each molecule. The coverage of each molecule in monolayers (ML) has been estimated by calculating the number of molecules on the surface for a given exposure, and comparing the size of an individual molecule to the density of the HOPG surface.

TPD experiments in both chambers were carried out using a linear heating rate of 0.50 ± 0.01 K s^{-1}, controlled by a Eurotherm 2408 interface. Desorbing gas phase species were monitored using either a HAL 201/PIC (chamber 1) or HAL 301/PIC (chamber 2) quadrupole mass spectrometer (Hiden Analytical). A range of masses was monitored for each molecule and all fragments exhibited the same behaviour. The most intense fragments are shown in the TPD spectra reported here: *m/z* 78 for benzene and *m/z* 91 for toluene, *p*-xylene and *o*-xylene. Both chambers were equipped with a Thermo-Nicolet FTIR spectrometer coupled to a liquid nitrogen cooled mercury cadmium telluride detector, which allowed RAIRS data to be recorded. Typically, a spectrum comprises the co-addition of 256 scans. A resolution of 2 cm^{-1} was used for xylene experiments, and 4 cm^{-1} for the benzene and toluene experiments. Lower resolution was used for the benzene and toluene experiments to give a better signal to noise ratio. RAIRS annealing experiments were carried out by raising the sample to the target temperature, holding for 3 minutes and then allowing the sample to cool down to base temperature before recording a spectrum. All experiments were repeated multiple times to ensure reproducibility.

Results and discussion

RAIRS data

The RAIR spectra of pure ices of 100 L_m of benzene, toluene, *p*-xylene and *o*-xylene adsorbed on HOPG between 25 and 30 K are shown in figure 2. For clarity the spectra have been split into three spectral regions which have different band intensities. All four molecules have common modes, although fewer modes are observed for benzene due to its simpler structure. The vibrational modes of the four molecules are detailed in tables 1 to 4, with assignments given by comparison with the literature.[39,42,43,46–50]

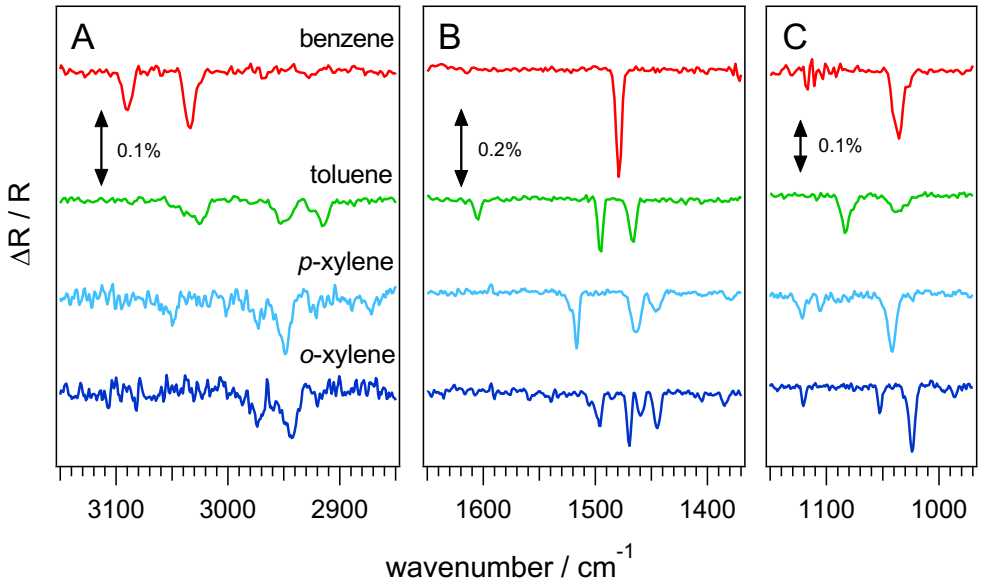

Figure 2. *RAIR spectra of 100 L_m benzene, toluene, p-xylene and o-xylene adsorbed on HOPG at 25 – 30 K. (A) shows the region between 3150 and 2850 cm^{-1}, (B) shows the region between 1650 and 1370 cm^{-1} and (C) shows the region between 1150 and 970 cm^{-1}.*

In the high wavenumber region, figure 2A, the aromatic CH stretching mode is observed at 3090 cm^{-1} for benzene (see tables 1-4 for assignments). It is redshifted to 3050 cm^{-1} in *p*-xylene and to 3026 cm^{-1} in toluene. This mode is not observed in *o*-xylene at base temperature, but appears after annealing to 120 K (see later). This is probably due to structural rearrangements in the *o*-xylene ice making this

mode observable after annealing. Methyl CH stretching modes are observed for toluene, *p*-xylene and *o*-xylene between 2900 and 3000 cm^{-1}. In figure 2B, only one band is observed for benzene, at 1479 cm^{-1}. This corresponds to the aromatic C=C stretching mode and is the most intense band observed at base temperature. Aromatic C=C stretching modes are also observed for toluene, *p*-xylene and *o*-xylene at slightly higher wavenumbers, 1486 to 1605 cm^{-1}. Methyl deformation and combination bands are also observed for toluene, *p*-xylene and *o*-xylene in figure 2B. Figure 2C shows CH in-plane deformations for each molecule between 1036 and 1121 cm^{-1}. Methyl rocking modes are also observed for toluene and the xylene isomers between 986 and 1041 cm^{-1}.

Annealing experiments were also performed to investigate the thermal ordering of the ices. Spectra were recorded at 10 K intervals from base temperature until all the ice desorbed from the HOPG surface. A range of exposures were studied for each molecule using RAIRS, and similar trends were observed for all exposures of benzene, toluene and *o*-xylene. However, for *p*-xylene exposure dependent differences were observed, discussed below.

Figure 3 shows RAIR spectra for 100 L_m benzene adsorbed on HOPG at 25 K and annealed to various temperatures. Table 1 gives the band assignments and their observed splitting with increasing temperature. No changes were observed in the spectra between 25 and 70 K. At 90 K several changes are observed. The aromatic CH stretch at 3090 cm^{-1} begins to split into two peaks, at 3091 and 3085 cm^{-1}, which become clearly defined at 110 K. Simultaneously the combination band at 3034 cm^{-1} starts to split at 90 K, leading to the formation of two distinct bands at 100 K, at 3037 and 3030 cm^{-1}. The aromatic C=C stretching mode at 1479 cm^{-1} doubles in intensity between 90 and 110 K. The band at 1036 cm^{-1} initially begins to broaden at 80 K, and then splits into two peaks, at 1040 and 1034 cm^{-1} at 110 K. All bands decrease in intensity at 130 K due to benzene desorption. By 140 K benzene has completely desorbed, in agreement with the TPD data described below.

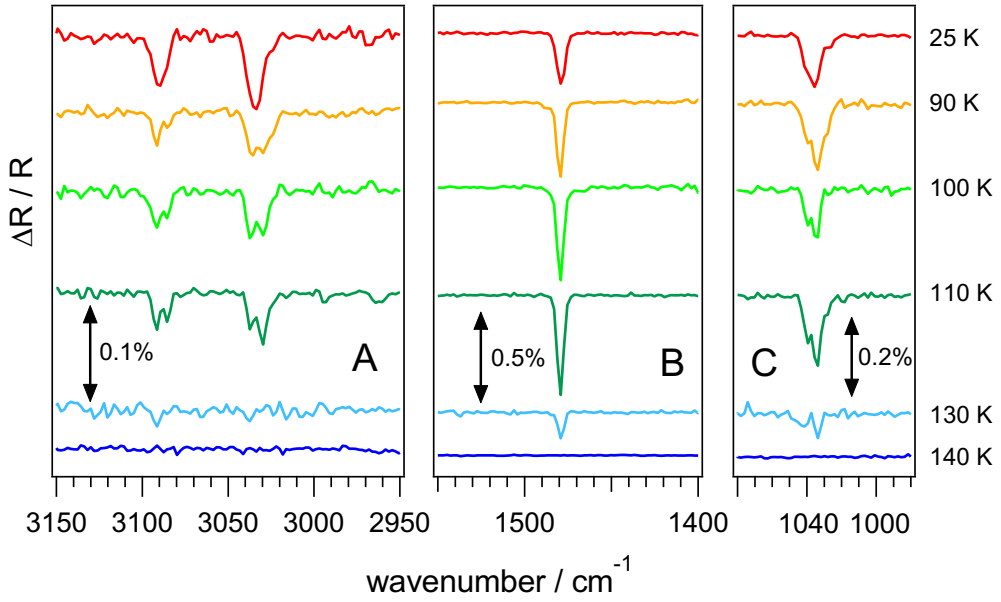

Figure 3. *RAIR spectra showing the effects of annealing 100 L_m of benzene adsorbed on HOPG at 25 K. (A) shows the 3150 - 2950 cm^{-1} region, (B) shows the 1550 - 1400 cm^{-1} region and (C) shows the 1080 - 980 cm^{-1} region. Annealing temperatures and band strengths are shown in the figure.*

Table 1. *RAIRS assignments for benzene adsorbed on HOPG at 25 K and thermally annealed to 110 K. Assignments are made by comparison with the literature.[46,47] Symbols: ν = stretching, δ = deformation.*

assignment	***Wavenumber / cm^{-1}***			
	HOPG at 25 K	*HOPG at 110 K*	*Ru at 14 K[46]*	*Si(111) at 77 K[47]*
ν(CH)$_{aromatic}$	3090	3091/3085	3095	3088
Combination band	3034	3037/3030	3043	3036
ν(C=C)$_{aromatic}$	1479	1479	1481	1480
δ(CH)$_{in\text{-}plane}$	1036	1040/1034	1038	1040

The sharpening and splitting of infrared bands upon heating is a sign of a structural change occurring in the ice. This change can be assigned to the transition of benzene from an amorphous to crystalline state. The crystallisation of benzene leads to the formation of in-phase and out-of-phase vibrational modes, which leads to the observed splitting in the RAIR spectra in figure 3. Similar splitting, assigned to crystallisation, has been observed for other molecules adsorbed on HOPG and subsequently

annealed.[51] A phase change has been observed for benzene adsorbed at 25 K on graphene coated Pt(111),[52] and at 45 K on Ru(001).[22] The coverage dependence of the crystallisation was also studied previously, with thicker films crystallising at lower temperatures.[22,53] Previous studies of the structure of multilayer crystalline benzene on Ru(001) show that it is oriented tilted on the surface.[22,23] This structural arrangement has also been demonstrated using neutron diffraction studies, which show a herringbone crystal packing.[54] It is likely that the same benzene crystal structure is formed here.

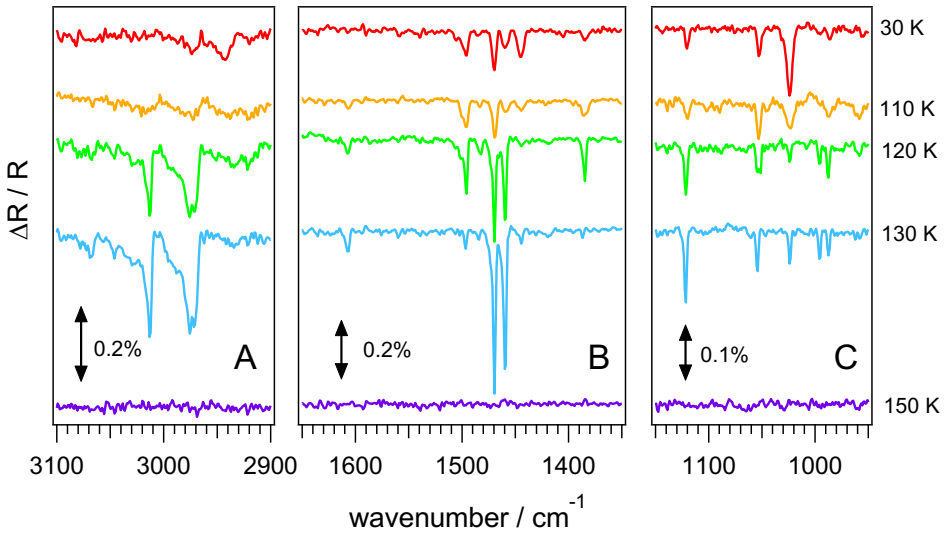

Figure 4. *RAIR spectra showing the effects of sequential annealing of a 100 L_m exposure of o-xylene adsorbed on HOPG at 30 K. (A) shows the region between 3100 and 2900 cm^{-1}, (B) shows the region between 1650 and 1350 cm^{-1} and (C) shows the region between 1150 and 950 cm^{-1}. Annealing temperatures and band strengths are shown in the figure.*

Figure 4 shows the RAIR annealing spectra for 100 L_m *o*-xylene absorbed on HOPG at 30 K, and table 2 lists the band assignments. Similar to benzene, no noticeable changes are observed on annealing *o*-xylene to 80 K. Between 80 and 110 K, minor changes occur to some bands seen in figure 4. The most significant changes occur when the *o*-xylene is annealed to 120 K, with several new bands appearing. These are the bands at 3013, 1607 and 996 cm^{-1}, which are assigned to the CH aromatic stretch, the C=C aromatic stretch and a CH_3 rocking mode respectively. Most of the bands in figure 4 also show an increase in intensity following annealing to 120 K, and continue to grow until 130 K. No further changes in the spectra occur at 140 K, and at 150 K desorption of *o*-xylene is complete.

Table 2. *RAIRS assignments for o-xylene adsorbed on HOPG at 30 K and annealed to 120 K. Assignments are made by comparison with the literature.* [39,43,48,55] *Symbols: ν = stretching, δ = deformation, ρ = rocking, s = symmetric, as = asymmetric.*

assignment	***Wavenumber / cm^{-1}***		
	HOPG at 30 K	*HOPG at 120 K*	*liquid*[55]
ν(CH)$_{aromatic}$	-	3013	3017
ν(CH)$_{methyl}$	2974	2976/2971	2971
ν(CH)$_{methyl}$	2943	-	2941
ν(C=C)$_{aromatic}$	-	1607	1607
ν(C=C)$_{aromatic}$	1496	1496	1496
ν(C=C)$_{aromatic}$	1486	1482	-
ν(C=C)$_{aromatic}$ and δ(CH$_3$) (as)	1470	1470	1468
ν(C=C)$_{aromatic}$ and δ(CH$_3$) (as)	1460	1460	1456
δ(CH$_3$) (as)	1445	1445	1443
δ(CH$_3$) (s)	1385	1385	1385
δ(CH)$_{in\text{-}plane}$	1121	1121	1120
δ(CH)$_{in\text{-}plane}$	1053	1054/1051	1053
ρ(CH$_3$)	1024	1024	1022
ρ(CH$_3$)	-	996	-
ρ(CH$_3$)	986	988	986

As for benzene, the changes observed in the RAIR spectra in figure 4 on annealing of *o*-xylene, *i.e.* increases in peak intensity and peak shifts, are attributed to structural changes and ordering within the ice. Neutron diffraction studies have suggested that crystal packing effects in *o*-xylene induce a high degree of strain in the phenyl ring.[56] The same study also discussed the potential for aromatic hydrogen bonding. It is likely that the same structural ordering of *o*-xylene occurs here on HOPG and hence the spectral changes observed in figure 4 are assigned to the crystallisation of *o*-xylene.

Figure 5 shows the RAIR annealing spectra of 100 L$_m$ *p*-xylene adsorbed on HOPG at 30 K and table 3 shows the assignments for the bands observed in this figure. Like *o*-xylene, these spectra also show

the growth in intensity of several bands as the annealing temperature is increased. Changes in the spectra in figure 5 are first observed at 100 and 110 K. Between 100 K and 130 K, the aromatic C=C stretching mode at 1517 cm^{-1} exhibits a large increase in intensity. At the same time, the peak shifts slightly to 1519 cm^{-1} and develops a high wavenumber shoulder at 1540 cm^{-1}. A small low wavenumber peak also appears at 1513 cm^{-1}. Shifts, detailed in table 3, and increases in intensity are also observed for the asymmetric CH_3 deformation band at 1464 cm^{-1}, the CH in-plane ring bending mode at 1121 cm^{-1}, and the CH_3 rocking mode at 1041 cm^{-1}. In the high wavenumber region (figure 5A), the bands at 3021 and 2999 cm^{-1} begin to grow at 100 K. All of the bands between 3050 and 2950 cm^{-1} grow between 100 and 140 K. All of the bands seen in figure 5 reach their maximum intensity at 140 K and at 150 K, *p*-xylene begins to desorb. All of the *p*-xylene has desorbed by 160 K, in agreement with TPD data (shown later).

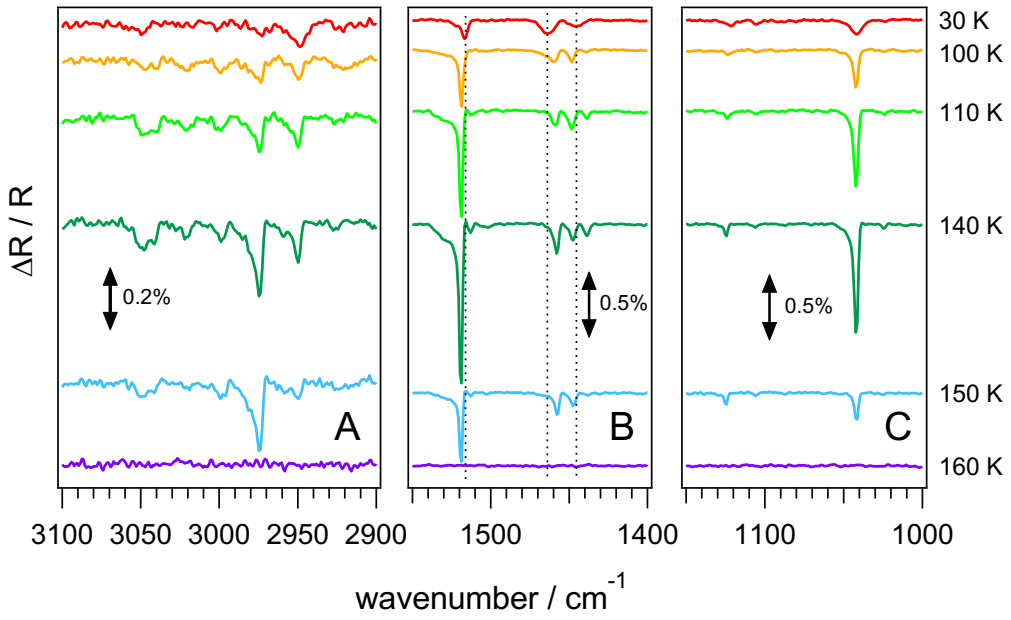

Figure 5. *RAIR spectra showing the effects of annealing 100 L_m of p-xylene adsorbed on HOPG at 30 K. (A) shows the region between 3100 and 2900 cm^{-1}, (B) shows the region between 1550 and 1400 cm^{-1} and (C) shows the region between 1150 and 1000 cm^{-1}. Annealing temperatures and band strengths are shown in the figure.*

Table 3. *RAIRS assignments for p-xylene adsorbed on HOPG at 30 K and annealed to 110 K. Assignments are made by comparison with the literature.[39,43,49] Symbols: ν = stretching, δ = deformation, ρ = rocking, as = asymmetric.*

assignment	***Wavenumber / cm^{-1}***		
	HOPG at 30 K	*HOPG at 110 K*	*liquid[49]*
ν(CH)$_{aromatic}$	3050	3050/3041	3044
ν(CH)$_{aromatic}$	-	3021	3017
ν(CH)$_{aromatic}$ or ν(CH)$_{methyl}$	-	2999	-
ν(CH)$_{methyl}$	2974	2974	2975
ν(CH)$_{methyl}$	2950	2950	2947
ν(C=C)$_{aromatic}$	1517	1519/1513	1529
δ(CH$_3$) (as)	1464	1458	1458
δ(CH$_3$) (as)	1445	1448/1439	1452
δ(CH) $_{in\text{-}plane}$	1121	1124	1120
δ(CH) $_{in\text{-}plane}$	1106	1106	-
ρ(CH$_3$)	1041	1043	1041

RAIR spectra for lower exposures of *p*-xylene (not shown) are the same at base temperature. However, annealing lower exposures of *p*-xylene shows differences when compared to the spectra seen in figure 5. RAIR spectra observed for 50 L_m *p*-xylene following annealing are shown in figure S1 in the supplementary material. These spectra do not show the same temperature dependent changes as seen in figure 5, and show different ratios of band intensities across the spectra as the sample is annealed.

The exposure and temperature dependent changes observed in the RAIR spectra of *p*-xylene (figure 5 and figure S1) indicate that several different processes are happening within the ice. Initial effects, seen for all bands and all exposures when the ice is annealed to 110 K and above, are attributed to ordering of the ice. For exposures less than 50 L_m, the RAIR spectra do not change on annealing above 110 K (figure S1), and therefore the ice desorbs in the ordered state. For exposures of 100 L_m and

above (figure 5), further changes are observed in the spectra following annealing to above 110 K. These further changes are assigned to complete crystallisation of the *p*-xylene ice before desorption. For exposures of *p*-xylene between 50 and 100 L_m the phase change only occurs when the ice is annealed to 150 K, as evidenced by a high temperature shoulder in the TPD spectra at these exposures (see later), showing that the phase changes occurs during desorption.

Experiments were also conducted for *p*-xylene adsorbed on HOPG at 120 K, for several exposures between 30 and 150 L_m. RAIR spectra of these ices recorded at base temperature without further annealing (not shown), show the same features as observed in the spectra for 100 L_m *p*-xylene at 110 K (figure 5). TPD traces from these experiments, discussed later, show only one peak with a higher desorption temperature. This indicates that when the ices are adsorbed at 120 K the phase change occurs regardless of the exposure. These results suggest that there is a barrier to forming crystalline *p*-xylene, and this is only overcome when either the exposure or the deposition temperature is sufficiently high. Exposure and temperature dependent crystallisation have also been observed for benzene[22] and thiophene.[57] This effect has not previously been observed for *p*-xylene. The crystal structure of *p*-xylene has been examined using neutron powder diffraction at 4.5 K. [58] A herringbone crystal packing, similar to benzene, has been observed for *p*-xylene. Hence, it is likely that *p*-xylene adopts this same crystal structure when adsorbed on the HOPG surface and annealed.

Annealing experiments were also conducted for toluene ices, as shown in figure S2 in the supplementary information. Very few changes were observed when compared to the base temperature toluene spectra seen in figure 2. The assignments of the toluene bands in figure 2 and figure S2 are detailed in table 4. All bands decrease in intensity following annealing to 130 K due to toluene beginning to desorb from the surface, and by 140 K it has completely desorbed. These observations are in agreement with TPD data (shown later) that show that multilayer toluene desorbs from the HOPG surface around 140 K.

Table 4. *RAIRS assignments for toluene adsorbed on HOPG at 25 K. Assignments are made by comparison with the literature.[42,50] Symbols: ν = stretching, δ = deformation, s = symmetric, as = asymmetric.*

assignment	***Wavenumber / cm^{-1}***	
	HOPG at 25 K	*Ni(111) at 110 K[42]*
ν(CH)$_{aromatic}$	3026	3027
ν(CH$_3$) (as)	2951	2922
ν(CH$_3$) (s)	2916	2876
ν(C=C)$_{aromatic}$	1605	1605
ν(C=C)$_{aromatic}$	1495	1495
ν(C=C)$_{aromatic}$ and δ(CH$_3$) (as) combination	1466	1464
δ(CH) $_{in\text{-}plane}$	1084	1082
ρ(CH$_3$)	1039	1030/1014

The lack of changes observed in the toluene RAIR spectra following annealing suggests that very little structural rearrangement of the molecules occurs upon heating. This is in contrast to the other molecules, which all show a dramatic change in the observed infrared bands upon annealing. This is also in contrast to the work of Coats *et al.*, who observed reorientation of multilayer toluene on Ni(111) when annealed to 132 K.[42] Previous work examining the glass transition temperature of toluene on Ni, using a heating rate of 5 K min^{-1}, found that it crystallises at 147 K.[59] The crystallisation temperature in both of these studies[42,59] is close to the desorption temperature observed in the experiments described here. It is hence likely that due to the higher heating rate used in our study, crystallisation does not occur before toluene desorbs. The lack of ordering and crystallisation observed for toluene may explain why the desorption temperature is not higher than that of benzene, despite toluene being a slightly larger molecule.

TPD data

The thermal desorption behaviour of low exposures (≤ 20 L_m) of benzene, toluene, *p*-xylene and *o*-xylene adsorbed on HOPG between 25 and 30 K is shown in figure 6. It can clearly be seen that the desorption of the four molecules is different at these exposures. Benzene and toluene behave similarly, however the xylene isomers show very different behaviour.

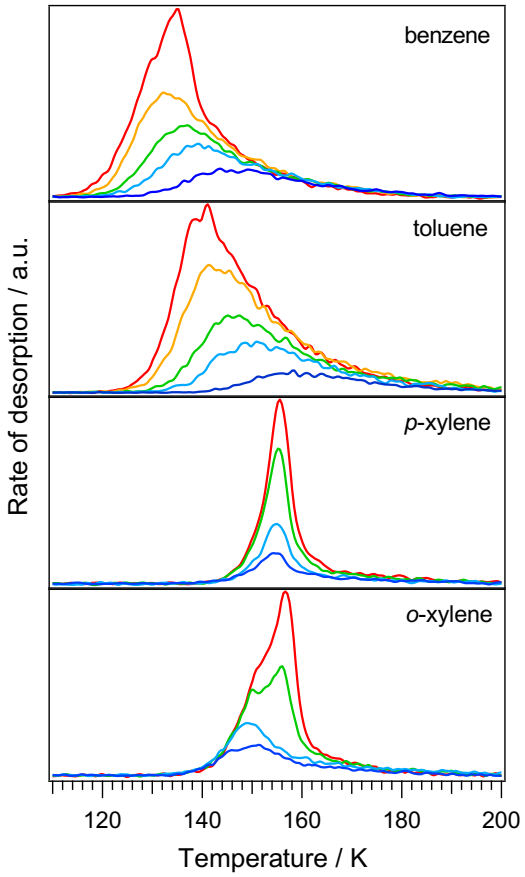

Figure 6. *TPD spectra of low coverages, approximately 0.2 to 1 ML, of benzene, toluene, p-xylene and o-xylene adsorbed on HOPG at 25 – 30 K. From the top: benzene exposures of 3, 5, 7, 10 and 15 L_m; toluene exposures of 3, 7, 10, 15 and 20 L_m; p-xylene exposures of 5, 7, 12 and 15 L_m; o-xylene exposures of 5, 10, 15 and 20 L_m.*

Figure 6 shows the TPD spectra of benzene and toluene between 3 and 15 L_m and 3 and 20 L_m respectively. TPD data for lower exposures of benzene, 0.3 – 2 L_m (not shown), were also recorded and show the same trends as observed for 3 – 15 L_m. Benzene and toluene show complex desorption

behaviour at these exposures, as seen in figure 6, with a very broad peak spanning a temperature range of over 40 K. As the exposure increases the desorption temperature decreases; for benzene the peak temperature changes from 164 K at 0.3 L_m to 132 K at 10 L_m, a difference of 32 K. For toluene this change is not as dramatic, with a desorption temperature of 158 K at 3 L_m to 139 K at 25 L_m. Concurrent with a decrease in desorption temperature, the peak shape also changes with increasing exposure. Initially, at exposures less than 3 L_m, it is almost symmetrical, however as the exposure is increased it develops into an asymmetric shape with a steeper leading edge and broad trailing edge extending to the same high temperatures as the lowest exposures.

Previous studies of benzene on amorphous silica (SiO_2),[30,31] Cu(111),[25] graphene/Cu and graphene/SiO_2 [32] have yielded similar TPD traces, with decreasing desorption temperature as the exposure increases, and extended trailing edges. The broad peak shape and decrease in desorption temperature have previously been attributed to repulsive lateral interactions between the adsorbed molecules on the surface.[25,32] Although benzene is apolar, the π-electron cloud can become polarised upon adsorption, leading to repulsions between molecules. In agreement with the observations in the literature[25,30–32] we assign the decreasing peak temperature, seen in figure 6 for both benzene and toluene, to the presence of repulsions between the adsorbed molecules. The same behaviour has also been observed for other nonpolar molecules, such as alkanes, both experimentally and in Monte Carlo simulations.[60–62]

The behaviour of the xylene isomers on HOPG at low exposures is noticeably different compared to benzene and toluene, as seen in figure 6. TPD traces for *p*-xylene show a single narrow symmetrical peak with a constant desorption temperature of 155 K, for exposures from 5 to 15 L_m. This feature is assigned to the desorption of physisorbed monolayer *p*-xylene, which is characterised by TPD spectra, of increasing exposure, that have a constant peak temperature and do not share leading edges. The desorption order, shown in table 5, is first order, confirming the assignment to monolayer desorption.

Low exposures of *o*-xylene on HOPG, give TPD spectra (figure 6) different to those of the other three molecules. At the lowest exposures, 5 and 10 L_m, a single peak, with non-shared leading edges, is observed at 150 K. This feature also has an elongated trailing edge, although it is not as extreme as the trailing edge observed for benzene and toluene. With increasing exposure a second peak grows into the spectrum at 156 K (15 L_m). The traces for 15 and 20 L_m share leading edges which are shifted to a slightly higher temperature than the lower exposures. The initial peak observed at 5 and 10 L_m is assigned to desorption of monolayer *o*-xylene. The peak that appears at 15 L_m could be due to the growth of a bilayer. Bilayers have also been observed in the TPD spectra of methyl formate[51] and ethanol.[63] If this assignment is correct, then it suggests that *o*-xylene does not wet the surface and instead forms islands. These would take the form firstly of 2-dimensional monolayer islands and then 3-dimensional monolayer and bilayer clusters.

As well as observing qualitative affects in TPD, the data can also be used to give kinetic parameters for desorption, including the desorption order, energy and pre-exponential factor. The desorption kinetic parameters for monolayer *p*-xylene (figure 6) have been calculated using leading edge analysis. This methodology is explained in detail elsewhere [64] and has been shown to provide good results for many molecules.[51,65] Using leading edge analysis, a desorption order for monolayer *p*-xylene of 0.92 ± 0.09 and a desorption energy of 51.0 ± 4.5 kJ mol^{-1} were determined, as shown in table 5. The pre-exponential factor was calculated to be $3.1 \times 10^{17 \pm 0.9}$ s^{-1} (first order units are used for simplicity). Typical pre-exponential factors for first order desorption are of the order of 10^{13} s^{-1} [64] and hence the pre-exponential factor obtained for *p*-xylene is larger than expected. This is most likely due to *p*-xylene being a relatively large molecule and therefore having greater differences in the molecular degrees of freedom in the adsorbed and desorbed states.[28,66,67] A previous DFT study calculated the adsorption energy of *p*-xylene on graphene to be between 53.1 and 71.3 kJ mol^{-1} dependent on the position, orientation and calculation used.[45] Our calculated value for monolayer *p*-xylene fits well within this range.

Table 5. *Desorption kinetic parameters for monolayer ices of benzene, toluene, p-xylene and o-xylene adsorbed on HOPG at 25 – 30 K. p-xylene parameters were calculated using leading edge analysis. Desorption orders and pre-exponential factors for benzene, toluene and o-xylene are assumed and desorption energies are calculated using Kinetiscope. A range of desorption energies are given for benzene and toluene, see figure 7. First order units are used for the pre-exponential factor for simplicity.*

	Desorption order (n)	***Desorption energy (E_{des}) / kJ mol^{-1}***	***Pre-exponential factor (ν) / s^{-1}***
Benzene	1	(51.0 – 41.3) ± 2	$10^{13 \pm 1}$
Toluene	1	(48.0 – 42.4) ± 2	$10^{13 \pm 1}$
p-xylene	0.92 ± 0.09	51.0 ± 4.5	$3.1 \times 10^{17 \pm 0.9}$
o-xylene	0.9 ± 0.1	49.8 ± 7.3	$10^{16 \pm 1}$

Due to the decreasing peak temperature for benzene and toluene, and the two peaks observed for *o*-xylene in figure 6, it is not possible to use leading edge analysis for these molecules. Hence to determine kinetic parameters for monolayer benzene, toluene and *o*-xylene desorption from HOPG the kinetics simulation program Kinetiscope (http://www.hinsberg.net/kinetiscope) was used. For the quantitative analysis of benzene and toluene, first order desorption (n=1) was assumed with a pre-exponential factor of 10^{13} s^{-1}, based on the method used by Thrower *et al.*[30] This method oversimplifies the desorption processes, but gives a good approximation of the kinetic parameters. Using these values, desorption profiles were simulated in Kinetiscope to give estimated desorption energies. These derived profiles were then compared with the experimental TPD traces to find the best fits (see figure S3 for an example of the fit quality) for the desorption energy for each exposure (0.3 – 15 L_m for benzene, 3 – 25 L_m for toluene). Figure 7 shows the desorption energies of sub-monolayer benzene and toluene as a function of exposure determined using this method. It can clearly be seen that the desorption energy is dependent on the exposure and decreases as the exposure increases. The

desorption energy of benzene decreases quickly from 0.5 to 5 L_m (51.0 to 42.0 kJ mol^{-1}), and then plateaus at 10 – 15 L_m (41.3 kJ mol^{-1}). The decrease in energy for toluene is not quite as dramatic, decreasing from 48.0 to 42.4 kJ mol^{-1} (3 to 25 L_m). Desorption profiles were also simulated using a range of pre-exponential factors, from 10^{12} to 10^{14} s^{-1}. This was found to have only a small effect on the determined desorption energy of ± 2 kJ mol^{-1}. These are the errors given in table 5, and shown as error bars in figure 7.

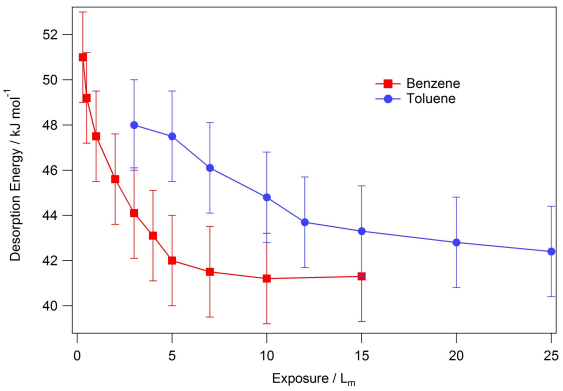

Figure 7. *Variation of desorption energies with exposure for sub-monolayer benzene (red squares) and toluene (blue circles) adsorbed on HOPG at 25 K. Values are determined using Kinetiscope from the TPD spectra in figure 6. Error bars result from the variation in pre-exponential factor in the simulations.*

Our results are in excellent agreement with data reported in the literature. Desorption energies for low exposures of benzene on amorphous silica range from 52 kJ mol^{-1} (for the lowest exposures) to 39.5 kJ mol^{-1}.[30] For graphene covered supports, a coverage-dependent binding energy for benzene has been observed ranging from 53 to 36 kJ mol^{-1}; this is also dependent on the support, with graphene/Ru(001) having the highest energies and graphene/SiO_2 the lowest.[32,33] Other studies do not show a coverage dependent desorption energy, however they still give values within the range determined in this study. These include the desorption of monolayer benzene from HOPG with a desorption energy of 48 ± 8 kJ mol^{-1},[27] and from graphene covered Pt(111), 54 ± 3 kJ mol^{-1}.[28] To the best of our knowledge, only one study has previously determined an experimental value for the desorption energy of monolayer toluene. A value of 68 ± 7 kJ mol^{-1} for toluene desorption from HOPG

was obtained using Redhead analysis.[26] This is much larger than the value determined here and it is most likely that this is due both to the higher desorption temperature, 179 K, that they observed for monolayer toluene and the higher value of their pre-exponential factor ($10^{19\pm2}$ s^{-1}). [26]

Kinetiscope was also used to simulate desorption profiles for monolayer *o*-xylene, with the resulting fits being of similar quality to those shown in figure S3 for benzene and toluene. Desorption orders and pre-exponential factors were varied in order to provide errors on the value of the desorption energy. Varying the pre-exponential factor by an order of magnitude or the desorption order by 0.1 gave energy differences of 2.8 kJ mol^{-1} and 4.5 kJ mol^{-1} respectively, as seen in table 5. The best fit values gave a desorption order of 0.9, desorption energy of 49.8 kJ mol^{-1} and a pre-exponential factor of 1×10^{16} s^{-1}. This desorption energy is 1.2 kJ mol^{-1} lower than that for monolayer *p*-xylene (table 5), which is reasonable given the slightly lower desorption temperature of *o*-xylene. The simulated desorption energy given in table 5 is slightly smaller than a DFT calculation of the adsorption energy of *o*-xylene on graphene, 57.1 kJ mol^{-1}.[45] The pre-exponential factor for *o*-xylene is of the same order of magnitude as that determined for *p*-xylene. This is an appropriate value given the relatively large size of *o*-xylene.

Figure 8 shows the TPD behaviour of the four molecules at exposures from 15 to 70 L_m for benzene and *p*-xylene, and 20 – 70 L_m for toluene and *o*-xylene. These exposures correspond to approximately 1 to 3.5 ML. The most striking difference between the four molecules in figure 8 is the difference in desorption temperature. The two xylene isomers desorb approximately 20 K higher than benzene and toluene.

The desorption of benzene (figure 8) shows a single peak at exposures of 20 L_m and higher. The desorption temperature remains roughly constant (136 K) between 15 and 30 L_m. The TPD spectra in this range have non-overlapping edges. These peaks are assigned to the transition between monolayer and multilayer benzene. For exposures of 30 L_m and above, the spectra share leading edges and the desorption temperature increases with increasing exposure. This trend continues for higher exposures

(figure S4 in the supplementary material). This behaviour is characteristic of zero order desorption kinetics and multilayer desorption. In the RAIRS experiments described earlier, it was observed that benzene crystallises at 100 K. Therefore the TPD spectra in figure 8 show the desorption of multilayer crystalline benzene.

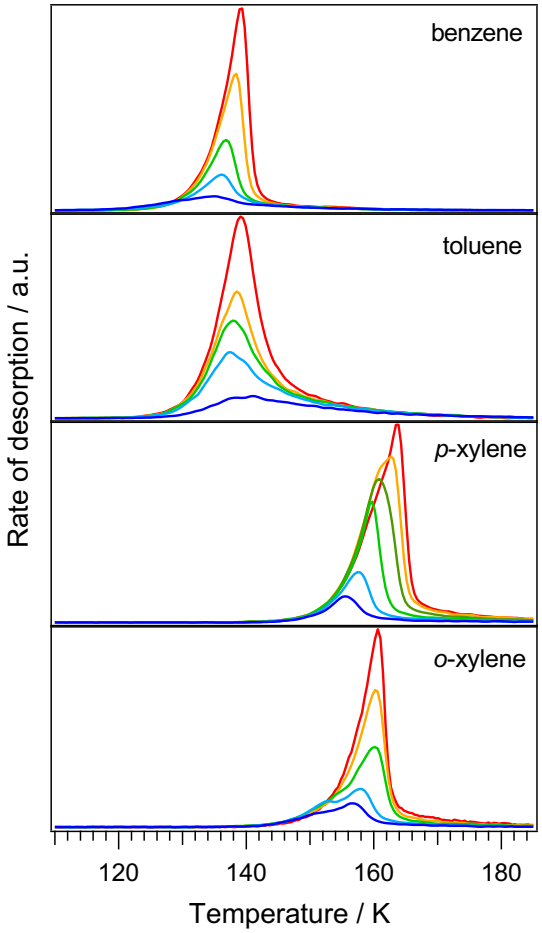

Figure 8. *TPD spectra of approximately 1 to 3.5 ML of benzene, toluene, p-xylene and o-xylene adsorbed on HOPG at 25 – 30 K. From the top: benzene exposures of 15, 20, 30, 50 and 70 L_m; toluene exposures of 20, 30, 40, 50 and 70 L_m; p-xylene exposures 15, 20, 40, 50, 60 and 70 L_m; o-xylene exposures of 20, 30, 50, 60 and 70 L_m.*

Toluene TPD spectra (figure 8) show similar behaviour to benzene at exposures between 20 and 70 L_m. However, the peak shape is asymmetric and has an elongated trailing edge, similar to its behaviour at lower exposures. The desorption temperature is comparable to benzene at the same exposures,

and is 139 K at 70 L_m. A continuation of multilayer desorption behaviour is observed for higher exposures, shown in figure S4. As no changes indicating ordering or crystallisation were observed in the annealing RAIR spectra for toluene, the TPD traces shown in figure 8 are assigned to the desorption of amorphous multilayer toluene.

The TPD traces of *p*-xylene between 15 and 40 L_m, shown in figure 8, consist of a single peak. These traces share leading edges and show a steady increase in desorption temperature with increasing exposure, from 156 K at 15 L_m to 160 K at 40 L_m. This peak can be assigned to the desorption of multilayer *p*-xylene. Between 50 and 70 L_m a high temperature shoulder appears on the TPD peak. Deviations from a single multilayer peak, such as shoulders on the TPD trace, have been observed for several molecules, including water,[68] and are often indications of restructuring happening in the ice during desorption. RAIRS experiments, discussed earlier, showed that for exposures of *p*-xylene up to 100 L_m, ordering occurs at 110 K. This is below the desorption temperature of 160 K observed in TPD experiments. For exposures up to 40 L_m, no further changes were observed in RAIR spectra and hence TPD traces for 15 to 40 L_m show desorption of this ordered state. For *p*-xylene exposures from 50 to 100 L_m, crystallisation of the ice occurs at 150 K, before desorption occurs. Hence, the phase change is observed as the shoulder in the TPD traces in figure 8. For exposures of 100 L_m, RAIR spectra showed that the phase change occurs at 110 K and therefore no shoulder is seen on the TPD trace at exposures greater than this (figure S4). TPD traces for *p*-xylene exposures of 100 L_m and above are hence assigned to the desorption of crystalline multilayer *p*-xylene.

TPD data were also recorded for *p*-xylene adsorbed at 120 K. These TPD traces (figure S5 in the supplementary information) display single peak multilayer spectra without a shoulder, with a desorption temperature 2 K higher than the ices adsorbed at 30 K. This corresponds to the desorption temperature of the high temperature shoulder in figure 8 for exposures over 50 L_m. When deposited at this elevated temperature, crystalline *p*-xylene ices are directly formed, as evidenced by RAIRS. This

confirms that the phase change is dependent on the exposure and also the temperature of deposition and annealing.

TPD traces for 20 to 70 L_m of *o*-xylene are shown in figure 8. The behaviour of *o*-xylene is in contrast to that of *p*-xylene at these exposures. Two peaks are observed for *o*-xylene exposures of 15 L_m, shown in figure 6, up to 50 L_m. This behaviour has tentatively been assigned to bilayer formation. The high temperature peak is dominant and grows at a greater rate than the low temperature peak. For exposures of 60 L_m and above, only the high temperature peak is observed. This peak increases in temperature with exposure, reaching 161 K at 70 L_m, and is similar to the desorption temperature of ordered multilayer *p*-xylene. Figure S4, in the supplementary material, shows the continuation of multilayer desorption behaviour for higher exposures up to 150 L_m. This high temperature peak is hence attributed to the desorption of multilayer crystalline *o*-xylene, as confirmed with RAIRS.

Quantitative analysis of the multilayer TPD spectra shown in figure 8 and figure S4 has also been performed using the leading edge methodology. Multilayer kinetic parameters for all four molecules on HOPG are given in table 6. These are the values for crystalline benzene, *p*-xylene and *o*-xylene, and amorphous toluene. As for the desorption temperatures, the desorption energies increase in the order benzene, toluene, *o*-xylene and finally *p*-xylene. These also show the same pairings; benzene and toluene have desorption energies of 45.5 and 47.6 kJ mol^{-1} respectively, and then there is a gap of almost 10 kJ mol^{-1} to the xylene isomers, 56.8 and 59.5 kJ mol^{-1} for *o*-xylene and *p*-xylene, respectively. The multilayer desorption energies for *p*-xylene and *o*-xylene, table 6, are higher than their equivalent monolayer desorption energies, shown in table 5. This is to be expected as the multilayer desorption temperatures are higher than their monolayer desorption temperatures. The determined desorption energies are in good agreement with enthalpies of sublimation reported in the literature. For benzene this value ranges from approximately 43 to 47 kJ mol^{-1}.[69] Other reported values for the enthalpy of sublimation are 43.1 kJ mol^{-1} for toluene,[70] 59.4 – 60.8 kJ mol^{-1} for *p*-xylene,[71,72] and 60.1 kJ mol^{-1} for *o*-xylene.[71]

Table 6. *Desorption kinetic parameters for multilayer ices of benzene, toluene, p-xylene and o-xylene adsorbed on HOPG at 25 – 30 K. For simplicity, zero order units are used for the pre-exponential factor.*

	Desorption order (n)	***Desorption energy (E_{des}) / kJ mol^{-1}***	***Pre-exponential factor (v) / molecules cm^{-2} s^{-1}***
Benzene	0.18 ± 0.06	45.5 ± 1.8	$2.6 \times 10^{29 \pm 2}$
Toluene	0.37 ± 0.04	47.6 ± 1.2	$3.3 \times 10^{27 \pm 0.3}$
p-xylene	0.14 ± 0.04	59.5 ± 1.7	$3.6 \times 10^{31 \pm 0.4}$
o-xylene	0.27 ± 0.05	56.8 ± 3.6	$1.1 \times 10^{29 \pm 0.7}$

Previously reported values for the desorption energy of multilayer benzene from a range of surfaces are comparable with our calculated energy. These include desorption energies of 46.6 ± 0.8 kJ mol^{-1} from SiO_2,[30] 48.5 ± 3.0 kJ mol^{-1} from Ru(001),[23] and 41.4 ± 0.9 kJ mol^{-1} from Cu(111).[25] Ulbricht *et al.* derived a value of 44 ± 7 kJ mol^{-1} for the desorption of multilayers of benzene from graphite,[26] although they assumed first order desorption kinetics, even for the multilayer. There are fewer experimental values for the desorption energy of multilayer toluene. In the same study by Ulbricht *et al.*, a value of 54 ± 6 kJ mol^{-1} for the desorption energy of multilayer toluene from graphite was derived.[26] This is higher than the desorption energy obtained in this work, although it does fit within the errors. To the best of our knowledge there are no experimental or theoretical literature desorption energy values for xylene isomers.

The desorption order expected for multilayers is zero, however for each of the molecules it is slightly elevated, from 0.14 for *p*-xylene to 0.37 for toluene, table 6. Fractional order desorption kinetics are also expected from the observation of non-coincident leading edges in the TPD spectra. This is especially clear for toluene in figure 8. As seen in table 6, the pre-exponential factor varies between 10^{27} and 10^{31} molecules cm^{-2} s^{-1} for toluene and *p*-xylene respectively. These values are typical for zero-order processes. There is a compensatory effect observed between the desorption order and pre-exponential factor, with a higher order resulting in a lower pre-exponential factor, and vice versa.

A previously reported value for the pre-exponential factor of multilayer benzene is $10^{29.7 \pm 1.0}$ molecules cm^{-2} s^{-1},[30] in very good agreement with our value of 2.6×10^{29} molecules cm^{-2} s^{-1}.

Comparison of the molecules

The results discussed above show how a small change in the molecular size can have a large impact on the desorption behaviour of small aromatic molecules. The addition of methyl groups affects both the polarity and the size of the molecule. At low exposures of benzene, repulsive intermolecular interactions are dominant. As described above, this is assigned to the polarisation of the π-electron cloud when it is adsorbed on the surface. It is observed that the addition of a methyl group to the benzene ring, forming toluene, results in similar desorption behaviour to benzene. The dipole moment of toluene does not seem to affect its behaviour at low exposures. However, when two methyl groups are attached to the benzene ring, forming xylene, a completely different behaviour is observed, which is also dependent on the relative positions of the methyl groups. *p*-xylene, which is apolar, shows well-behaved first order desorption kinetics. As evidenced by the high desorption energy, it also binds strongly to the HOPG surface, possibly overcoming any repulsive interactions that might exist. Conversely, *o*-xylene, which has the largest dipole moment of the molecules in this study, exhibits islanding and bilayer formation, albeit at a similar temperature and desorption energy to *p*-xylene. The differences between the monolayer behaviour of the xylene isomers shows that the contribution of the dipole moment is important.

The behaviour observed for multilayer exposures is in contrast to that for monolayer exposures. TPD data show that only the size of the molecule has an effect on the desorption behaviour, with the larger molecules, *p*-xylene and *o*-xylene, desorbing at higher temperatures with higher desorption energies. This size effect has also been observed previously for the thermal desorption of a series of *n*-alkanes from graphite.[73] RAIRS data are complementary to the TPD data and provide details on the ordering of the ice. The two apolar molecules, benzene and *p*-xylene, desorb as multilayer crystalline ices. They

are both thought to form a herringbone crystal structure. Multilayer *o*-xylene also desorbs as a crystalline ice, however, multilayer toluene desorbs as an amorphous ice.

Conclusions

In this paper we have reported a comparative study of the desorption behaviour of benzene, toluene *p*-xylene and *o*-xylene adsorbed on HOPG at ≤ 30 K. At the lower exposures studied, where monolayer desorption is observed, the interactions between adsorbates are dependent on their size, polarisability and dipole moment. Benzene and toluene behave similarly with repulsive adsorbate-adsorbate interactions, whereas the xylene isomers behave differently. This is due to their larger size, and interaction with the HOPG surface, outweighing any polarisation effects. The desorption temperatures for the multilayer systems are affected more by molecular size, with the xylene isomers desorbing approximately 20 K higher than benzene and toluene. RAIRS data show that benzene, *p*-xylene and *o*-xylene form crystalline structures as they are annealed to higher temperatures. This is in contrast to toluene which does not show any signs of ordering. This may explain why the desorption temperature of toluene is similar to benzene. *p*-xylene also shows an inhibition to forming a full crystalline state dependent on the exposure and adsorption temperature.

Desorption energies have been calculated for all four molecules for both monolayer and multilayer systems. The monolayer desorption energy for benzene and toluene is dependent on the exposure, decreasing as the exposure increases. Multilayer desorption energies increase with molecular size, in the order benzene, toluene, *o*-xylene, *p*-xylene.

Supplementary Material

See supplementary material for figures S1 – S5. Figure S1- RAIR spectra showing the effects of sequential annealing of a 50 L_m exposure of *p*-xylene adsorbed on HOPG at 30 K. Figure S2- RAIR spectra showing the adsorption of a 100 L_m exposure of toluene adsorbed on HOPG at 25 K, and after annealing to 70 K. Figure S3 – Comparison of experimental and simulated TPD spectra for low

exposures of benzene and toluene. Figure S4- TPD spectra of multilayer exposures (2.8 to 8 ML) of benzene, toluene, *p*-xylene and *o*-xylene adsorbed on HOPG at 25 – 30 K. Figure S5- TPD spectra of multilayer exposures of *p*-xylene, dosed on HOPG at 120 K.

Acknowledgements

This work is funded by the STFC under Grant No. ST/M000869/1. The STFC also funded a post-doctoral fellowship for T.L.S. under this grant code. J.W.S. thanks the University of Sussex for funding.

References

[1] W.M. Haynes, editor , *CRC Handbook of Chemistry and Physics*, 94th ed. (CRC Press, Boca Raton, Florida, 2013).

[2] T.M. Sack, D.H. Steele, K. Hammerstrom, and J. Remmers, Atmos. Environ. Part A. Gen. Top. **26**, 1063 (1992).

[3] A. Zalel, Yuval, and D.M. Broday, Environ. Pollut. **156**, 553 (2008).

[4] P.A. Tesner and S. V. Shurupov, Combust. Sci. Technol. **105**, 147 (1995).

[5] H.M. Daly and A.B. Horn, Phys. Chem. Chem. Phys. **11**, 1069 (2009).

[6] G.D.J. Guerrero Peña, M.M. Alrefaai, S.Y. Yang, A. Raj, J.L. Brito, S. Stephen, T. Anjana, V. Pillai, A. Al Shoaibi, and S.H. Chung, Combust. Flame **172**, 1 (2016).

[7] J.R. Odum, T.P.W. Jungkamp, R.J. Griffin, H.J.L. Forstner, R.C. Flagan, and J.H. Seinfeld, Environ. Sci. Technol. **31**, 1890 (1997).

[8] R. Atkinson, Atmos. Environ. **34**, 2063 (2000).

[9] C. Song, K. Na, B. Warren, Q. Malloy, and D.R. Cocker, Environ. Sci. Technol. **41**, 7403 (2007).

[10] Y. Zhou, H. Zhang, H.M. Parikh, E.H. Chen, W. Rattanavaraha, E.P. Rosen, W. Wang, and R.M. Kamens, Atmos. Environ. **45**, 3882 (2011).

[11] M.I. Konggidinata, B. Chao, Q. Lian, R. Subramaniam, M. Zappi, and D.D. Gang, J. Hazard. Mater. **336**,

249 (2017).

[12] F. V Hackbarth, V.J.P. Vilar, G.B. De Souza, S.M.A.G.U. de Souza, and A.A.U. de Souza, Adsorption **20**, 577 (2014).

[13] S. Morales-Torres, F. Carrasco-Marín, A. Pérez-Cadenas, and F. Maldonado-Hódar, Catalysts **5**, 774 (2015).

[14] D. Fairén-Jiménez, F. Carrasco-Marín, and C. Moreno-Castilla, Langmuir **23**, 10095 (2007).

[15] J. Cernicharo, A.M. Heras, A.G.G.M. Tielens, J.R. Pardo, F. Herpin, M. Guélin, and L.B.F.M. Waters, Astrophys. J. **546**, L123 (2001).

[16] J. Bernard-Salas, E. Peeters, G.C. Sloan, J. Cami, S. Guiles, and J.R. Houck, Astrophys. J. **652**, L29 (2006).

[17] B.B. Dangi, D.S.N. Parker, R.I. Kaiser, A. Jamal, and A.M. Mebel, Angew. Chemie Int. Ed. **52**, 7186 (2013).

[18] R.I. Kaiser, T.L. Nguyen, T.N. Le, and A.M. Mebel, Astrophys. J. **561**, 858 (2001).

[19] E. Herbst, Astrophys. J. **366**, 133 (1991).

[20] P. Ehrenfreund and S.B. Charnley, Annu. Rev. Astron. Astrophys **38**, 427 (2000).

[21] A.G.G.M. Tielens, Annu. Rev. Astron. Astrophys **46**, 289 (2008).

[22] P. Jakob and D. Menzel, J. Chem. Phys. **105**, 3838 (1996).

[23] P. Jakob and D. Menzel, Surf. Sci. **220**, 70 (1989).

[24] J. Günster, J. Stultz, S. Krischok, and D.. Goodman, Chem. Phys. Lett. **306**, 335 (1999).

[25] M. Xi, M.X. Yang, S.K. Jo, B.E. Bent, and P. Stevens, J. Chem. Phys. **101**, 9122 (1994).

[26] H. Ulbricht, R. Zacharia, N. Cindir, and T. Hertel, Carbon **44**, 2931 (2006).

[27] R. Zacharia, H. Ulbricht, and T. Hertel, Phys. Rev. B **69**, 155406 (2004).

[28] R.S. Smith and B.D. Kay, J. Phys. Chem. B **122**, 587 (2018).

[29] M. Komarneni, A. Sand, J. Goering, U. Burghaus, M. Lu, L. Monica Veca, and Y.-P. Sun, Chem. Phys. Lett. **476**, 227 (2009).

[30] J.D. Thrower, M.P. Collings, F.J.M. Rutten, and M.R.S. McCoustra, Mon. Not. R. Astron. Soc **394**, 1510

(2009).

[31] J.D. Thrower, M.P. Collings, F.J.M. Rutten, and M.R.S. McCoustra, J. Chem. Phys. **131**, 244711 (2009).

[32] A. Chakradhar, N. Sivapragasam, M.T. Nayakasinghe, and U. Burghaus, J. Vac. Sci. Technol. A **34**, 21402 (2016).

[33] A. Chakradhar, K. Trettel, and U. Burghaus, Chem. Phys. Lett. **590**, 146 (2013).

[34] C. Xu, J.W. Peck, and B.E. Koel, J. Am. Chem. Soc. **115**, 751 (1993).

[35] A.L. Marsh, D.J. Burnett, D.A. Fischer, and J.L. Gland, J. Phys. Chem. B **107**, 12472 (2003).

[36] M. Saeys, J.W. Thybaut, M. Neurock, and G.B. Marin, Mol. Phys. **102**, 267 (2004).

[37] N. Klomkliang, D.D. Do, and D. Nicholson, Ind. Eng. Chem. Res. **51**, 5320 (2012).

[38] V.R. Choudhary, K.R. Srinivasan, and A.P. Singh, Zeolites **10**, 16 (1990).

[39] O. Marie, F. Thibault-Starzyk, and P. Massiani, J. Catal. **230**, 28 (2005).

[40] T. Ncube, K.S. Kumar Reddy, A. Al Shoaibi, and C. Srinivasakannan, Energy & Fuels **31**, 1882 (2017).

[41] H. Rauscher, P. Jakob, D. Menzel, and D.R. Lloyd, Surf. Sci. **256**, 27 (1991).

[42] A.M. Coats, E. Cooper, and R. Raval, Surf. Sci. **307**–**309**, 89 (1994).

[43] D.E. Wilk, C.D. Stanners, Y.R. Shen, and G.A. Somorjai, Surf. Sci. **280**, 298 (1993).

[44] D.G. Klarup, E.L. Muetterties, and A.M. Stacy, Langmuir **1**, 764 (1985).

[45] Ø. Borck and E. Schröder, Surf. Sci. **664**, 162 (2017).

[46] R. Ruiterkamp, Z. Peeters, M.H. Moore, R.L. Hudson, and P. Ehrenfreund, Astron. Astrophys **440**, 391 (2005).

[47] G. Strazzulla and G. Baratta, Astron. Astrophys **241**, 310 (1991).

[48] J.H.S. Green, Spectrochim. Acta Part A Mol. Spectrosc. **26**, 1913 (1970).

[49] J.H.S. Green, Spectrochim. Acta Part A Mol. Spectrosc. **26**, 1503 (1970).

[50] G.E. Douberly, A.M. Ricks, P.V.R. Schleyer, and M.A. Duncan, J. Phys. Chem. A **112**, 4869 (2008).

[51] D.J. Burke, F. Puletti, P.M. Woods, S. Viti, B. Slater, and W.A. Brown, J. Phys. Chem. A **119**, 6837 (2015).

[52] R.A. May, R.S. Smith, and B.D. Kay, J. Phys. Chem. A **117**, 11881 (2013).

[53] P. Swiderek and H. Winterling, Chem. Phys. **229**, 295 (1998).

[54] S.K. Nayak, R. Sathishkumar, and T.N.G. Row, CrystEngComm **12**, 3112 (2010).

[55] R. Lindenmaier, N.K. Scharko, R.G. Tonkyn, K.T. Nguyen, S.D. Williams, and T.J. Johnson, J. Mol. Struct. **1149**, 332 (2017).

[56] R.M. Ibberson, C. Morrison, and M. Prager, Chem. Commun. 539 (2000).

[57] H. Haberkern, S. Haq, and P. Swiderek, Surf. Sci. **490**, 160 (2001).

[58] R.M. Ibberson, W.I.F. David, S. Parsons, M. Prager, and K. Shankland, J. Mol. Struct. **524**, 121 (2000).

[59] R. Souda, J. Phys. Chem. B **114**, 10734 (2010).

[60] S.L. Tait, Z. Dohnálek, C.T. Campbell, and B.D. Kay, J. Chem. Phys. **125**, 234308 (2006).

[61] S. Funk, T. Nurkic, and U. Burghaus, Appl. Surf. Sci. **253**, 4860 (2007).

[62] E. Kadossov and U. Burghaus, Surf. Sci. **603**, 2494 (2009).

[63] D.J. Burke, A.J. Wolff, J.L. Edridge, and W.A. Brown, J. Chem. Phys. **128**, 104702 (2008).

[64] D.J. Burke and W.A. Brown, Phys. Chem. Chem. Phys. **12**, 5947 (2010).

[65] S.A. Ayling, D.J. Burke, T.L. Salter, and W.A. Brown, RSC Adv. **7**, 51621 (2017).

[66] S.L. Tait, Z. Dohnálek, C.T. Campbell, and B.D. Kay, J. Chem. Phys. **122**, 164708 (2005).

[67] K.A. Fichthorn and R.A. Miron, Phys. Rev. Lett. **89**, 196103 (2002).

[68] H.J. Fraser, M.P. Collings, M.R.S. McCoustra, and D.A. Williams, Mon. Not. R. Astron. Soc **327**, 1165 (2001).

[69] J.S. Chickos and W.E. Acree, J. Phys. Chem. Ref. Data **31**, 537 (2002).

[70] C. Lenchitz and R.W. Velicky, J. Chem. Eng. Data **15**, 401 (1970).

[71] W. Hessler and W. Lichtenstein, Wissenschaftliche Zeitschrift Der Wilhelm-Pieck Univ. Rostich **35**, 27 (1986).

[72] R.M. Stephenson and S. Malanowski, *Handbook of the Thermodynamics of Organic Compounds* (Springer Netherlands, Dordrecht, 1987).

[73] K.R. Paserba and A.J. Gellman, J. Chem. Phys. **115**, 6737 (2001).